LAWRENCE
LIVERMORE
NATIONAL
LABORATORY

UCRL-TR-218345

Constraints on the Nature of Terrestrial Core-Forming Melts: Ultra-High Pressure Transport Property Measurements and X-Ray Computed Tomography Final Report

J. J. Roberts, J. H. Kinney, F. J. Ryerson

January 24, 2006

This work was performed under the auspices of the U.S. Department of Energy by University of California, Lawrence Livermore National Laboratory under Contract W-7405-Eng-48.

Constraints On The Nature Of Terrestrial Core-Forming Melts: Ultra-High Pressure Transport Property Measurements And X-Ray Computed Tomography

04-LW-077

FINAL REPORT

J. J. Roberts[1], J.H. Kinney[2], and F. J. Ryerson[1]

Atmospheric, Earth and Environment Department[1]
Mechanical Engineering Department[2]

Principal Investigator's Contact Information:
J. J. Roberts L-201
Atmospheric, Earth, and Energy Department
Phone: (925)-422-7108
Email: roberts17@llnl.gov

Abstract

A key issue in models of planetary core formation is the interconnectness and potential percolation of iron-sulfide melts in contact with silicates at high temperature and pressure. To address this issue an integrated study of the electrical conductivity-texture-permeability relationships of olivine-sulfide partial-melt samples was performed. This work has application to the interpretation of high conductivity zones in the Earth as revealed by electromagnetic studies and to the origin and development of the Earth's core. The project consisted of three main tasks. 1) Synthesis and characterization of olivine-sulfide partial-melts. 2) Electrical conductivity measurements of the partial-melt and the individual melt and crystalline phases. 3) X-ray microtomographic determination of the 3-D structure and interconnectedness of the melt phase. The results are used to determine a model of permeability of a partially molten solid that incorporates the melt distribution, a goal that has never before been achieved. Material synthesis was accomplished in the piston cylinder apparatus and electrical conductivity measurements were performed at one atmosphere. X-ray computed tomography was performed on recovered samples at the ALS. This work makes use of and further enhances LLNL's strengths in high-pressure material properties, x-ray micro- and nanoscale imaging and development of transport theory.

Table of Contents

I. Background and Specific Aims

For our two-year (FY2004-FY2005) LDRD project, "Constraints On The Nature Of Terrestrial Core-Forming Melts: Ultra-High Pressure Transport Property Measurements And X-Ray Computed Tomography," we advanced the hypothesis that careful synthesis, and characterization of olivine-sulfide partial-melts and physical property measurements could constrain models of core formation in terrestrial planets. We proposed to accomplish the following specific tasks:

1) Synthesize texturally-equilibrated olivine-sulfide partial-melts of appropriate chemistry with a range of melt content.
2) Develop procedures to measure the electrical conductivity of the run products in one-atmosphere chemically-controlled high-temperature environments.
3) Attempt to extend the measurements to in situ high P and T.
4) Image the run products using x-ray computed micro-tomography (XRCT).
5) Determine permeability using a lattice-Boltzmann simulation.
6) Present findings at international conferences and submit papers to high quality journals.

This final report details our accomplishments during the proposal period from October 1, 2003 to September 30, 2005.

I.a Scientific basis for the project

A central question in planetary science is how metallic cores of terrestrial planets and planetesimals form. Many models of planetary core formation rely on coalescing of large planetesimals with pre-formed metallic cores[3,6]. One mechanism by which these bodies might form metallic cores is through the percolation of liquid metal through a crystalline olivine matrix[7,8,9,10], a mechanism also required by some models involving non-pre-differentiated planetesimals[3,6,9]. The permeability of liquid Fe-Ni-S melts within an olivine matrix is critical in determining whether core formation proceeds by percolation of metallic liquid through a solid crystalline matrix, or by separation of immiscible metal within a planetary-scale magma ocean[10].

The distribution of Fe-Ni-S melt in an olivine matrix is dependent on the wetting angle between the melt and olivine. The wetting angle for these systems is controlled by a number of factors including chemical composition, fugacity of oxygen (f_{O2}) and sulfur concentration, temperature and pressure[11,12]. Whether or not a particular composition is wetting also depends on the cation/anion ratio; anion-rich compositions have lower dihedral angles than anion-poor compositions. Gaetani and Grove[13] demonstrated that, at f_{O2}s of the upper mantle, anion-rich compositions exist that are wetting.

The percolation threshold (i.e., the critical melt volume required to form an infinite, continuously connected melt) is expected to vary depending on composition and wetting angle[6]. Above the percolation threshold, believed to be roughly 6% by volume for dihedral angles of 100° [6,14,15], an interconnected melt yields high permeability, below this threshold isolated melt pockets (non-wetting) or tubules, interconnected along three-grain edges (wetting), result in negligible permeability at low melt volume fractions. Estimates of permeability, however, are widely variable: five orders of magnitude disparities below the percolation threshold, and more than two orders of magnitude above the percolation threshold.

Uncertainty in the value of permeability in the Fe-Ni-S-olivine system stems from the difficulties associated with direct experimental determinations. Instead, the permeability must be inferred, either from statistical models based on the microstructure, or from empirical models that relate permeability to electrical conductivity, although, to our knowledge, electrical conductivity has not been used to estimate permeability in this system. The universal approach, therefore, has been to infer permeability through a Kozeny-Carman relation of the form $k = \alpha d^2 \phi^n$, where k is the permeability, α is a numeric constant related to the shape of the interconnected pores ($1/24\pi$), d is related to the grain size of the olivine, ϕ is the volume fraction of the melt, and n is a scaling exponent that depends on the assumed form of the flow model. Various investigators have proposed scaling exponents that range from n = 1-3.8[1,2,3,5,16].

Here, we determine an independent measure of the permeability that does not depend upon any presumed scaling law.

II. Accomplishments

Overall the project was very successful with each task accomplished or with demonstrated significant progress. Thus far the work has resulted in 7 conference presentations, two journal articles (one submitted, one published), and two additional journal articles still to be submitted. Two summer students were supported by the project, one of who is the lead author on the published paper. Here we highlight specifically the x-ray micro CT imaging, lattice-Boltzmann determinations of permeability and a significant finding, the scaling exponent for permeability in these systems.

II a: Imaging of FeS partial-melts

The quenched specimens were imaged on the dedicated tomography beamline 8.3.2 at the Advanced Light Source (Lawrence Berkeley National Laboratory). Radiographic images of the specimen (Figure 1) were recorded as it was rotated in 0.5 degree increments. Four images were signal averaged at each orientation; the exposure time ranged from 100 10 400 msec per image. As the vertical beam dimension is only 2.5 mm, the specimen was scanned in sections. After each scan, the specimen was translated vertically by the precise amount of the beam height, and then rescanned. The scans can then be tiled together to form one complete image.

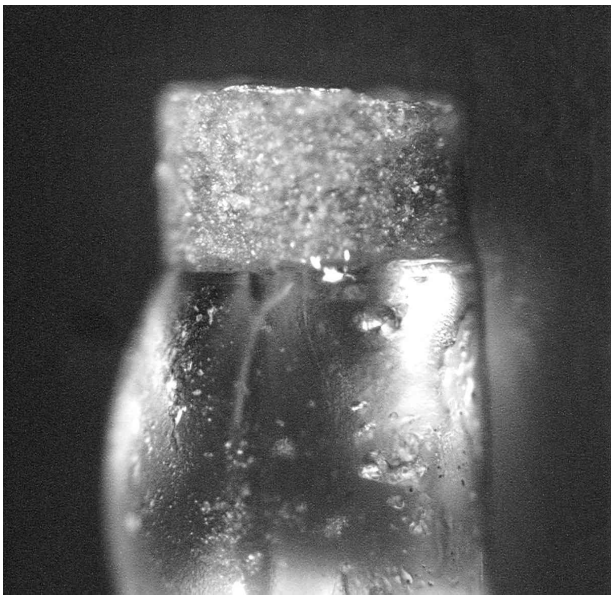

Figure 1: The sample was mounted on a rotating goniometer, positioned so that the x-ray beam passed through the centrum. Sample is 0.7 mm diameter.

Three-dimensional images of the olivine microstructure were reconstructed at 1.6 micron spatial resolution using a parallel-beam Fourier filtered back projection algorithm. The reconstructions required about 2 hours on a dual processor, 2.4 GHz Pentium 4. The final reconstructed volume consisted of approximately 2 x 10^{10} volume elements (voxels). Subsets on the order of 10^6 to 10^7 volume elements were used for lattice-Boltzmann simulations.

Due to its greater x-ray opacity the Fe-Ni-S melt was easily distinguished from the olivine matrix allowing the use of a single, global image threshold to isolate the melt pockets at concentrations above 5%. For melt fractions below 5%, however, single voxel noise broke the connectivity of several of the smallest conducting channels; for these melt concentrations, a local threshold, which takes into account nearest neighbors, was used. There was no discernable difference between the local and global thresholds when compared at melt concentrations above 5%.

Percolating and non-percolating melt fractions develop strikingly different 3-dimensional morphologies (Figure 2). As predicted for percolating compositions, the morphology consists of melt pockets interconnected by thin tubules occupying three-grain junctions. In contrast, the non-percolating melt forms isolated pockets without interconnecting tubules.

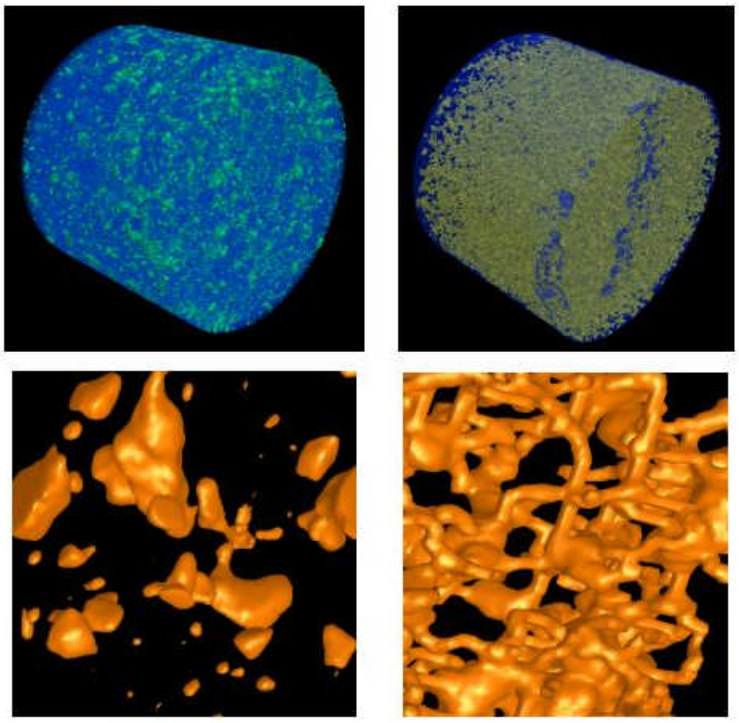

Figure 2: Three dimensional images of metallic iron-sulfide partial-melts in an olivine matrix. Left images are of FeS-olivine, right images are FeNiS-olivine melts. Top images show general melt distribution in cylindrical volumes approximately 0.7 mm diameter and 1.0 mm length. Bottom images are higher magnification show the melt morphology in greater detail. The two systems, Ni-absent and Ni-containing, for melt fractions below and above what is believed to be the percolation threshold (4-6 % vol) show distinctive differences in melt distribution, interconnectivity, and melt pocket morphology. The non-percolating composition forms isolated melt pockets that; in contrast, the percolating composition forms melt pockets that remain interconnected by small tubules.

The additional images (Figure 3-5) show a sample of the range of melt interconnected textures encountered for these systems and highlights the differences between the Ni-bearing and Ni-absent melts.

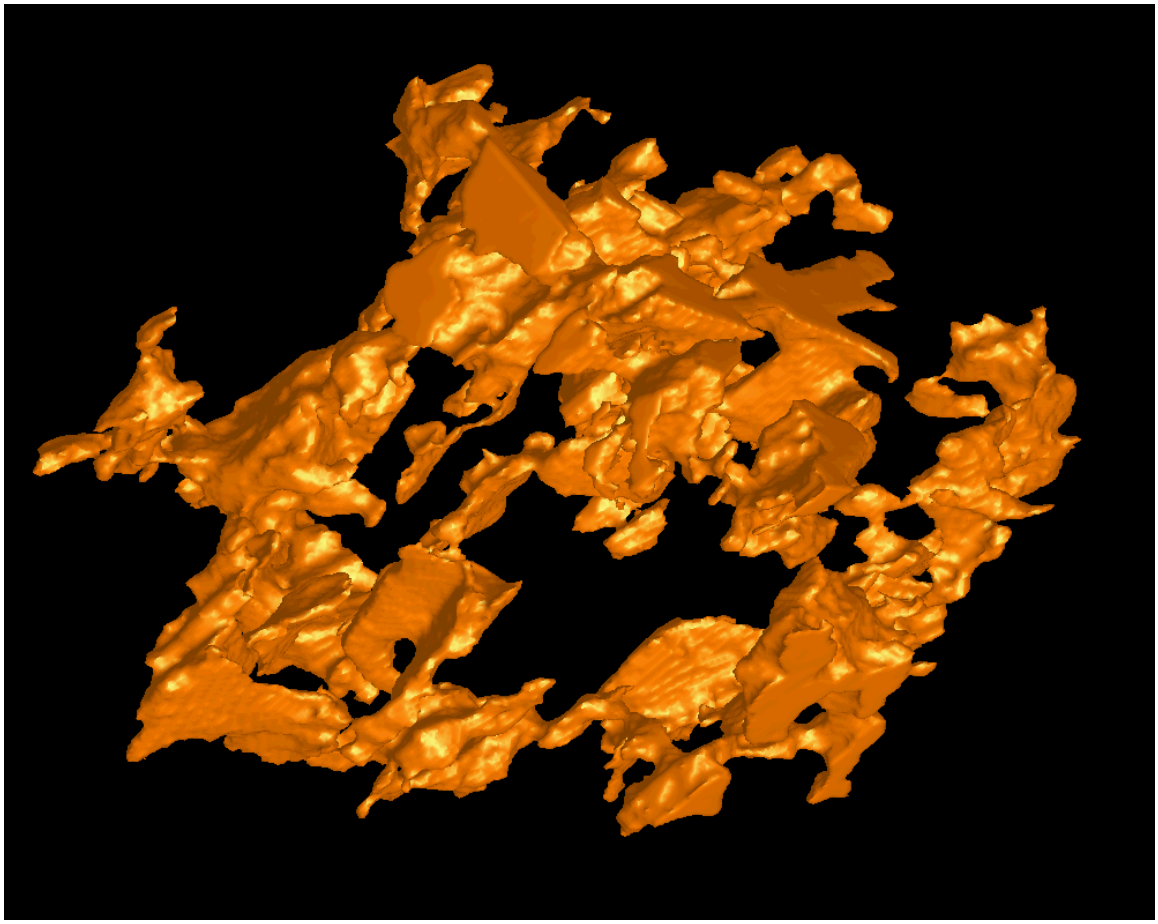

Figure 3: Rendered image of FeS with a melt fraction of 12%. 160 x 160 x 160 microns.

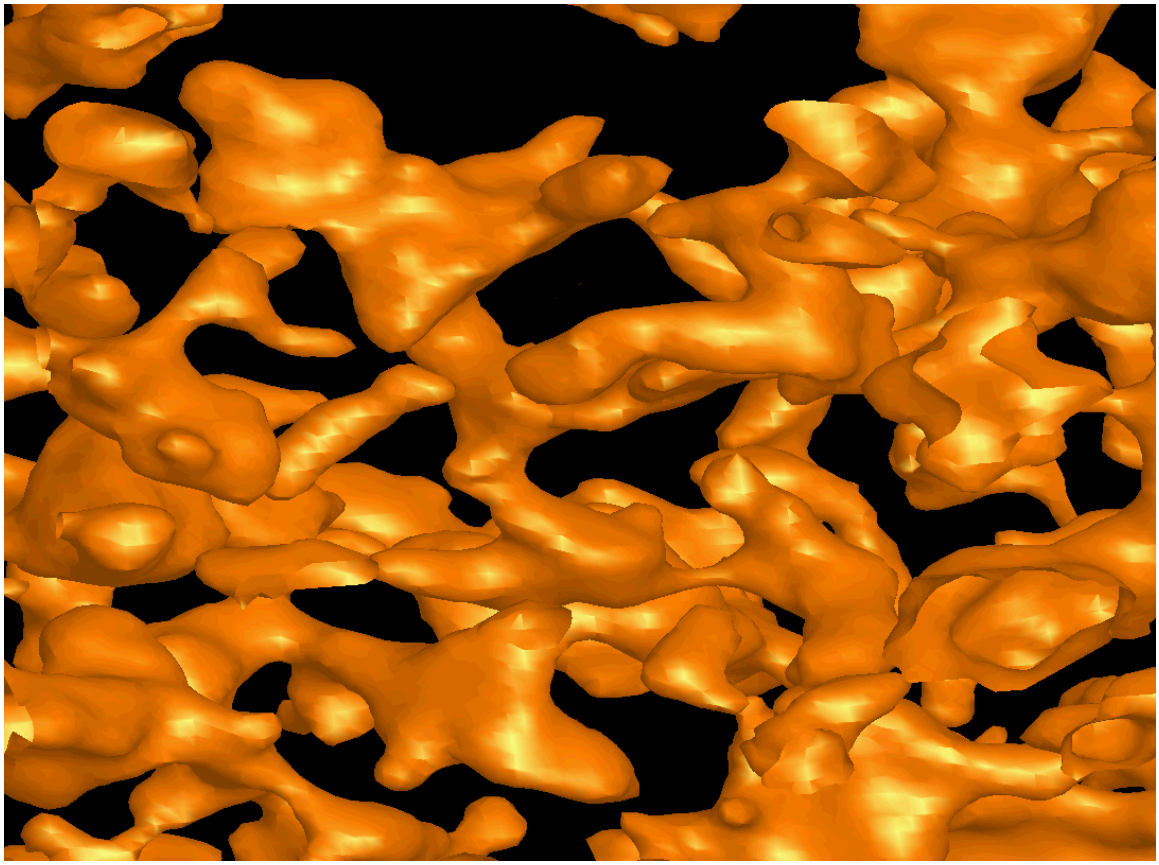

Figure 4: Rendered image of ($Fe_{92.5}Ni7_{.5}$)S with a melt fraction of 12%, well above the percolation threshold. Approximately 200 micron cubic volume. Compare texture to Figure 3.

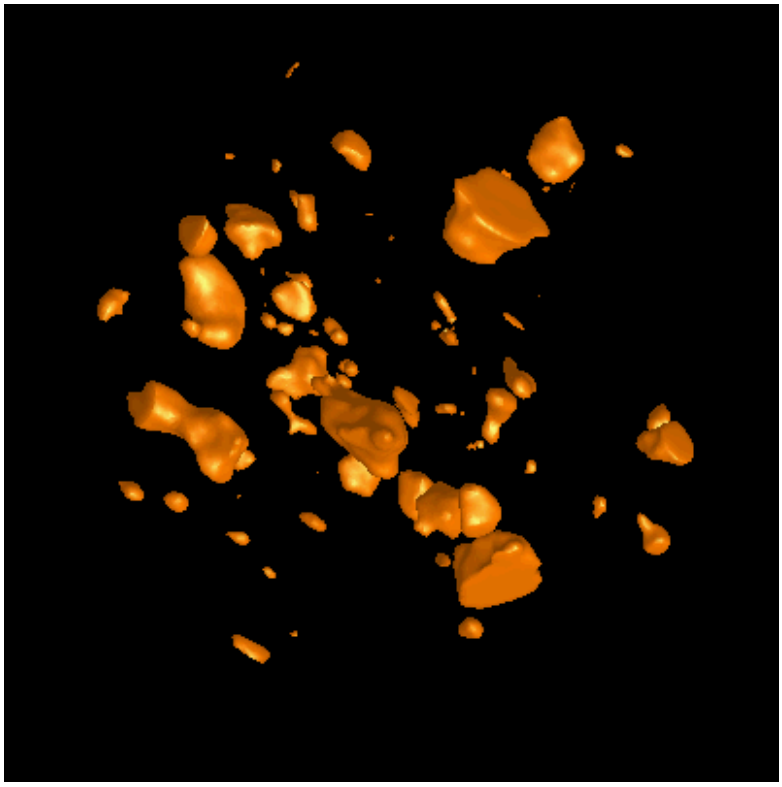

Figure 5: Rendered image of FeS with a melt fraction of 4% showing isolated melt. 160 x 160 x 160 microns.

II b: Lattice-Boltzmann simulations of permeability

The lattice-Boltzmann method (LB) is a discrete formulation of the Boltzmann equation on a grid or lattice and can be used to solve two- and three- dimensional hydraulic permeability problems[17,18]. For this study x-ray CMT will provide the model of the pore space used in the calculations. LB has been applied successfully to diverse fluid flow problems[19,20]. It is especially useful for flow problems that involve complex geometries because the boundary conditions are easily implemented.

The Boltzmann equation is a fundamental equation from kinetic theory and statistical mechanics that describes the state of the fluid in a continuous field:

$$\frac{\partial n}{\partial t} + \upsilon \cdot \nabla n = \Omega(n, n) \,. \qquad (7)$$

Here, n is the single particle velocity distribution function, v is the velocity of the fluid and Ω(n,n) is the collision operator, which in rigorous form is an integral expression. A

rough estimate for the collision integral, known as the BGK (Bhatnagar-Gross-Krook) operator, can be used[21]. If Eq. (7) is discretized in space, time, and velocity, the lattice-Boltzmann equation is:

$$n_i(x + c_i, t+1) = \Omega(n_i(x_i,t)) + n_i(x,t). \tag{8}$$

Here n_i is the i^{th} portion of the single particle velocity distribution function particle density at position x in the i^{th} direction at time, t, and c_i are the discretized local velocities[22,23,24]. The lattice-Boltzmann equation considers particle distributions on lattice nodes instead of individual particles. By restricting the distribution function to particles on a lattice, a discrete approximation to the Navier-Stokes equations can be rigorously derived[25]. As the grid becomes infinitely small, the lattice-Boltzmann algorithm reproduces the incompressible Navier-Stokes equations[23]. One advantage of the lattice-Boltzmann method is that implementing physically realistic boundary conditions in complex geometries is more simplistic.

The full lattice-Boltzmann method can be written as:

$$n_i\left(x + c_i, t + \tau\right) = n_i\left(x,t\right) - \frac{n_i\left(x,t\right) - n_i^{eq}\left(x,t\right)}{\tau} \tag{9}$$

Here τ is the relaxation time, x is the position in space on the lattice, c_i is the lattice speed in the i^{th} direction and as shown in Eq. (7), we use the linearized collision operator.

To use the LB algorithm to solve hydraulic flow problems we employ an equi-spaced square lattice. For three-dimensional flow, both the 15 and 19 lattice velocity models are used, and particles on the lattice are restricted to moving only in the direction of neighboring grid points. For low Reynolds number flows, both models yield nearly identical results[18]. For the permeability calculations in this study, only the final, steady-state flow field is of interest. Many implementations of the LB method and codes exist. We are using two codes developed at Lawrence Livermore National Laboratory (LLNL). One by Bosl and one by Clague (i.e., Bosl et al., 1998; Clague et al., 2000). Both codes

have been benchmarked and provide reliable results. The codes have also been parallelized and run on LLNL's MCR. An additional advantage of the existing codes is that flow vectors at each point in the pore space are known. This information is powerful because it can show which pores or pathways dominate the flow path and which pores are stagnant or near stagnant (Figure 6). This sample is a fused glass bead sample with a porosity of about 19%. The permeability was measured in the laboratory to be ~760 mD. Preliminary lattice-Boltzmann calculations yield a permeability ranging between 700 and 1000 mD, depending on scale and flow direction.

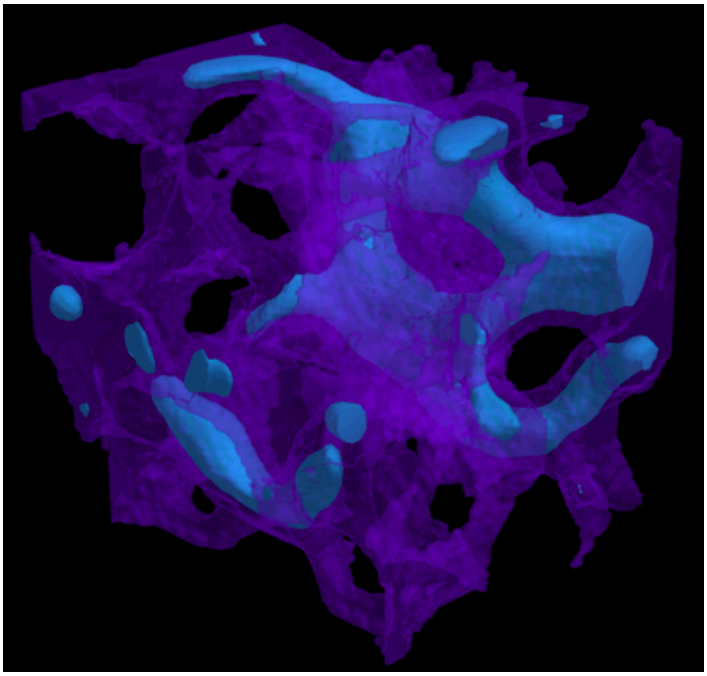

Figure 6. Three-dimensional rendered image of the pore volume of a fused glass bead sample with ~19% porosity. Scale is ~ 1 mm on each side and the spatial resolution is 11 microns. Grains are not shown, the purple or light shades are low flow regions and the blue or brighter shades represent high-flow regions as determined by lattice-Boltzmann simulation. X-ray CMT performed at the Advanced Light Source beamline 8.3.2.

The three-dimensional images of the melt structures were discretized into lattices for solution of the Stokes flow equation using the LB solver.[20,21] Calculations were performed on representative cubic volumes (roughly between 250 to 500 microns on edge) from the interiors of the specimens. The maximum size of the cubes was limited by

the presence of cracks created during the specimen quenching. The permeability was calculated along each of three orthogonal directions.

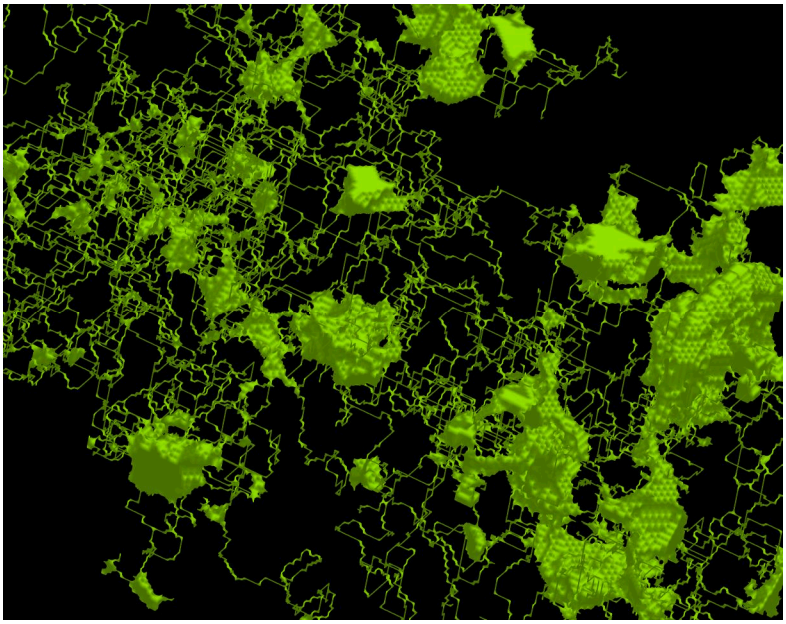

Figure 7: Partially skeletonized volume showing large pores and interconnecting melt tubules. 350 x 300 x 250 microns.

II c: Determination of the scaling exponent for permeability

The permeability is graphed in Figure 8 as a function of the melt concentration. For comparison, we have included model predictions proposed by other researchers. The scatter in the data reflects combinations of small specimen size and differences in pore morphology. The model described by Faul[2], with a scaling exponent of 3.0, is an upper bound to all of our calculated permeabilities. Unanticipated, our data is in better agreement with the scaling exponent of 3.8, which was proposed by Lockner and Evans[5] to explain changes in pore structure upon densification of quartz powders. Lockner and Evans modeled the pore morphology as spheres interconnected by cylindrical tubules; the non-integral scaling exponent is a result of a transition during uniform densification from a sphere-dominant morphology to cylindrical pore structures.

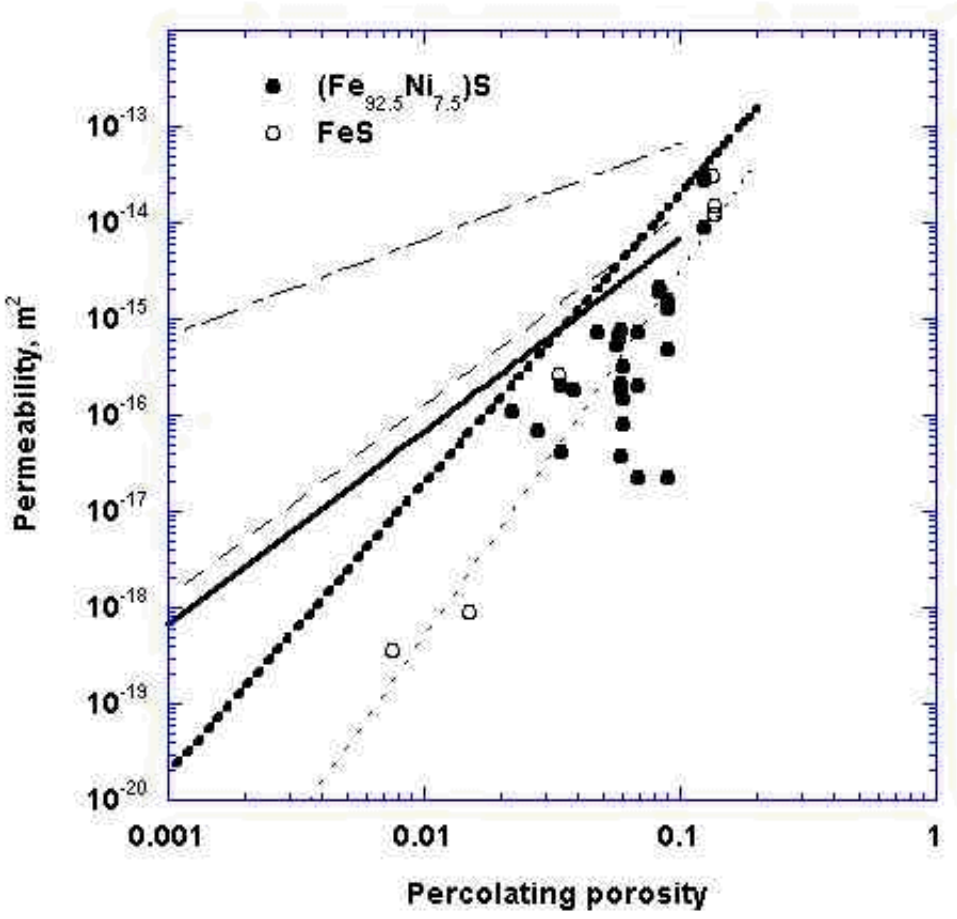

Figure 8: Permeability as a function of percolating porosity as determined by lattice-Boltzmann simulations of x-ray CT volumes for $(Fe_{92.5}Ni_{7.5})S$ (filled symbols) and FeS (open symbols). Lines represent permeability predicted by various models using the equation $k = \alpha d^2 \phi^n$ with α and n 3000 and 2^4 (solid line), 3000 and 1^1 (dash-dot), 1600 and 2^{15} (long dash) and 100 and 3^2 (heavy dot) for a grain size of 45 μm. The short dash line represents the model by Lockner and Evans[5], which consists of spheres intersected by straight tubes. The Ni-bearing samples appear more wetting then the FeS samples and thus a model using porosity to an exponent of 3 bests represents the upper bound of permeability. The FeS samples are not fully interconnected until the melt fraction approaches ~0.1 (Figure 9). The permeability appears better represented by the Lockner and Evans model that utilizes an exponent of 3.8.

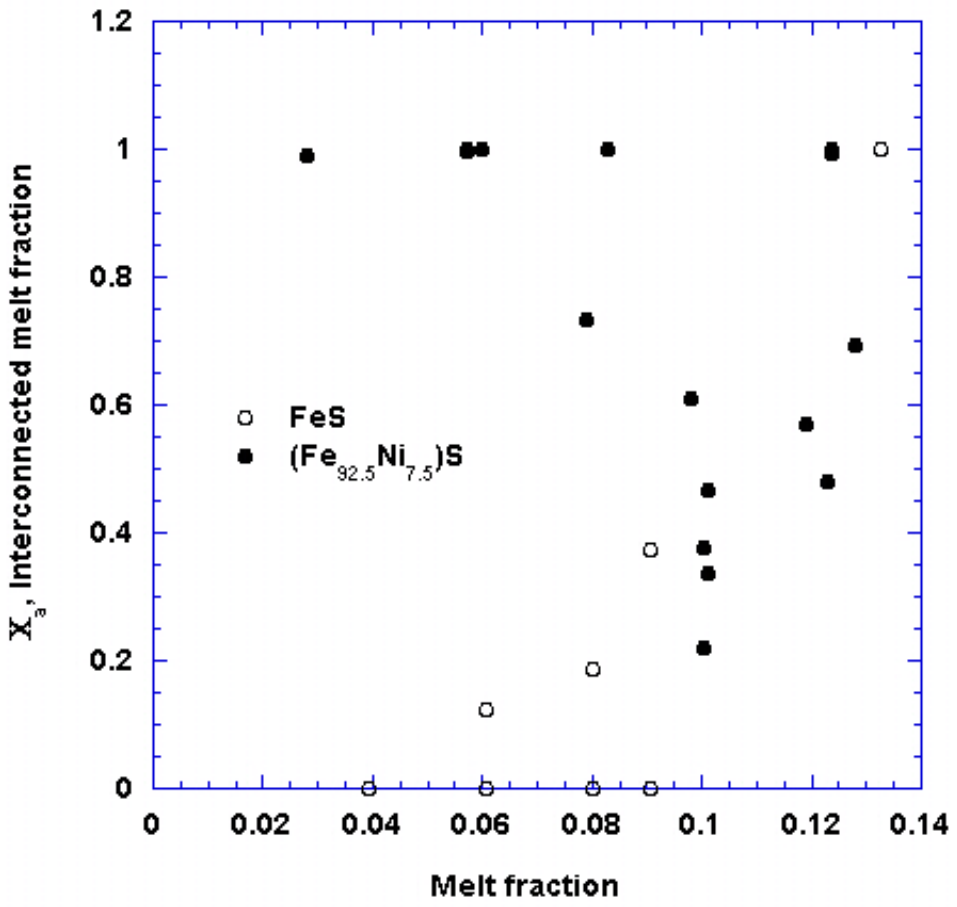

Figure 9: Interconnected melt fraction versus total melt fraction for all samples and sub-volumes. Filled symbols are Ni-bearing and open circles are FeS. Ni-bearing melt can be nearly fully interconnected at relatively low total melt fractions. FeS (Ni-absent) samples only interconnect fully at much higher melt fractions. Though it is possible that Ni might affect the wetting angle of the melt, and thereby lower the percolation threshold, we believe it more likely that the enhanced x-ray contrast provided by the Ni allows us to detect melt channels at lower concentration. The large scatter in the data reflects the difficulty in determining a percolation threshold in small sample volumes; a true percolation threshold can only be established in systems that are large enough to be considered "infinite."

II c: Constraints on core formation models

The present results allow a direct calculation of the migration rate in planetesimals and terrestrial planets. The migration rate of a metallic melt depends on the

density difference between sulfide melt and olivine ($\Delta\rho \sim 2.10^3$ kg/m^3), gravitational acceleration (g), permeability (k) and melt viscosity ($\eta \sim 10^{-2}$ Pa·s.[11] Accordingly:

$$v = \frac{k\Delta\rho g}{\eta}$$

With the scaling exponent 3.8, a grain size of 1 mm, and the permeability as determined from the Kozeny-Carman relation, the melt migration rate is approximately 5 m/year for a fraction melt of 0.1 and a planetesimal with a radius of 100 km (g = 0.1 ms^{-2}). Iron-rich cores apparently formed in these types of objects within about 3 million years.[29] Therefore, we conclude that permeable flow is a viable mechanism for core formation.

There was no difference in scaling between Ni and non-Ni formulations of the melts. However, the two systems appeared to have different melt morphologies: the percolation threshold of Ni-bearing FeS partial-melts was lower than that of FeS (Figure 3). Near percolation in the non-Ni formulations, only a small fraction of the total melt was interconnected. We observed a large number of isolated melt pockets surrounded by melt free grain boundaries for FeS. In contrast, melt commonly occurred on grain boundaries with the addition of Ni, thereby allowing percolation for melt concentrations lower than 6 % (volume). We do not expect that the addition of Ni changes the wetting angle significantly; indeed, our limited observations of the dihedral angles in these specimens were about 80^o (s.d. 20^o). It is believed that the percolation threshold is between 3-5 percent (Yoshino observed 6% for $Fe_{58}S_{42}$[27,28]). Here, the percolation threshold for FeS partial-melts appears to lie between 5 and 10 percent. However, the Ni-containing melts appear to have no clearly defined threshold. We speculate that the small addition of Ni increases the radiographic contrast sufficiently to allow detection of much smaller volumes of melt. This enhancement of contrast might explain the differences in the melt morphologies at the lowest melt concentrations.

III. Peer Reviewed Publications

Du Frane, W. L., J. J. Roberts, D. A. Toffelmier and J. A. Tyburczy, Anisotropy of electrical conductivity in dry olivine*, Geophys. Res. Lett*., 32, L24315, 2005, UCRL-JRNL-211347.

Roberts, J.J., J. Siebert, F. J. Ryerson, and J. H. Kinney, Determination of Olivine- Fe-S Partial Melt Permeability: Implications for Planetary Core Formation, Science, submitted, 2006, UCRL-JRNL-216014.

Conference Proceedings and Abstracts:

Roberts, J.J., J. H. Kinney, J. Siebert, and F. J. Ryerson, Permeability of Olivine-FeS Partial-Melts Based on Tomographic X-ray Imaging, Eos Trans. AGU, 86(52), Fall Meet. Suppl., Abstract MR13A-0073, 2005, UCRL-ABS-214980.

Du Frane, W. D., J. A. Tyburczy, J. J. Roberts, and D. A. Toffelmier, Anisotropic and Isotropic Effective Medium Olivine Models, Fall Meet. Suppl., Abstract GP41B-0874, 2005, UCRL-ABS-214900.

Wright, H. M., J. J. Roberts, and K. V. Cashman, Pore Structure of Pumice: Comparison Between Laboratory Measurements and X-Ray Tomographic Image Analysis Eos Trans. AGU, 86(52), Fall Meet. Suppl., Abstract V42A-06, 2005, UCRL-ABS-214899.

Kinney, J. H., and J. J. Roberts, Using Image Analysis to Determine Permeability in Otherwise Unmeasurable Systems, Center for Advanced Signal and Image Sciences Workshop, Livermore, CA, 2005, UCRL-ABS-216570.

Roberts, J. J., S. Mei, J. H. Kinney, and F. J. Ryerson, Electrical Properties of Olivine and Olivine-Sulfide Partial Melts: Constraints on the nature of terrestrial core-forming melts, *Eos Trans. AGU, 86*(18), Jt. Assem. Suppl., Abstract V51A-09, 2005, UCRL-ABS-209514.

Du Frane, W.D., J J Roberts, S Constable, D A Toffelmier, J A Tyburczy, Anisotropy of Point Defect Mechanisms and Electrical Conduction in Single Crystal Olivine, *Eos Trans. AGU*, Fall Meet. Suppl., Abstract GP13A-07, 2004, UCRL-ABS-206406.

Roberts, J.J., R. Ryerson, J. Kinney and B. Bosl, Electrical Properties Of Olivine-FeS Partial-Melts, Western Pacific Geophysics Meeting, Honolulu, HI., 16-20 August, 2004, UCRL-ABS-203509.

IV: Collaborations

IV a. Arizona State University

A long term collaboration has been established with Professor J. Tyburczy of Arizona State University. Through this project his graduate student, Wyatt Du Frane, came to LLNL. His role was to set-up, test, and calibrate the one-atmosphere gas mixing furnace and electrical conductivity measurements. For the calibration process he performed measurements on oriented dry olivine. The measurements were of sufficient quality to warrant publication and with subsequent defect modeling formed the basis of his M.S. thesis. The P.I. of this LDRD project (Jeff Roberts) served as his mentor and was officially on his graduate defense committee.

IV a. University of Oregon

A result of this project and our interest in x-ray imaging and permeability calculations led to a new collaboration with Professor Kathy Cashman of Oregon State University. Her Ph.D. student, Heather Wright, came to LLNL as a summer student in 2004 and 2005. Her role was the establishment of standard procedures used in x-ray CT data collection, image processing and the calculation of transport properties both through LB simulations and laboratory measurements. We expect her work on this project will produce an additional high quality peer-reviewed journal article, a news article in Eos, and constitutes a chapter in her dissertation. Ms. Wright is a superb scientist expected to finish her Ph.D. in June 2006. We are currently exploring the possibilities of a post-doctoral position at LLNL beginning summer 2006.

References

1. Riley, G. N., & Kohlstedt, D. L. Kinetics of melt migration in upper mantle-type rocks, *Earth Planet. Sci. Lett.*, **105**, 500–521 (1991)
2. Faul, U. H. Permeability of partially molten upper mantle rocks from experiments and percolation theory. *J. Geophys. Res*. **102**, 10299-10311 (1997)

3. Rushmer, T., Minarik, W. G. & Taylor, G. J. Physical processes of core formation. Origin of the Earth and Moon, (eds. Canup, R. M. & Righter, K.), pp. 227-242, Univ. Arizona Press, Tucson, AZ, (2000)
4. McKenzie, D. Some remarks on the movement of small fractions in the mantle, *Earth Planet. Sci. Lett.*, **95**, 53–72 (1989)
5. Lockner, D. & Evans, B. Densification of quartz powder and reduction of conductivity at 700 °C, *J. Geophys. Res.*, **100**, 13,081-13,092 (1995)
6. Stevenson, D. J., Fluid dynamics of core formation, Origins of the Earth, (eds. Newsom, H.E. & Jones, J. H.), pp. 231-249, Oxford University, New York, (1990)
7. Shannon, M.C. & Agee, C. B. Percolation of core melts at lower mantle conditions, *Science,* **280**, 1059-1061 (1998)
8. Terasaki, H., Frost, D. J., Rubie, D.C. & Langenhorst, F. The effect of oxygen and sulphur on the dihedral angle between Fe-O-S melt and silicate minerals at high pressure: Implications for Martian core formation, *Earth Planetary Sci. Lett.,* **232**, 379-392 (2005)
9. Jacobsen S. B., The Hf-W isotopic system and the origin of the earth and moon *Ann. Rev. Earth Planet. Sci.,* **33**, 531-570 (2005)
10. Holzheid, A., Schmitz, M. D. & Grove, T. L. Textural equilibria of iron sulfide liquids in partly molten silicate aggregates and their relevance to core formation scenarios, *J. Geophys. Res.*, **105**, 13,555-13,567 (2000)
11. Rubie, D. C., Melosh, H. J., Reid, J. E., Liebske, C. & Righter, K. Mechanism of metal-silicate equilibration in the terrestrial magma ocean, *Earth Planet. Sci. Lett.*, **205**, 239-255 (2003)
12. Rose, L. A. & Brenan, J. M. Wetting properties of Fe-Ni-Co-Cu-O-S melts against olivine: Implications for sulfide melt mobility, *Econ. Geol.,* **96**, 145-157 (2001)
13. Gaetani, G. A. & Grove, T. L. Wetting of mantle olivine by sulfide melt: Implications for Re/Os ratios in mantle peridotite and late-stage core formation, *Earth Planetary Sci. Lett.,* **169**, 147-163 (1999)

14. Bruhn, D., Groebner, N. & Kohlstedt, D. L. An interconnected network of core-forming melts produced by shear deformation, *Nature,* **403**, 883-886 (2000)
15. von Bargen, N. & Waff, H. S. Permeabilities, interfacial areas and curvatures of partially molten systems: Results of numerical computations of equilibrium microstructures, *J. Geophys. Res.,* **91**, 9261–9276, (1986)
16. Roberts, J. J. & Tyburczy, J. A. Partial-melt electrical conductivity: Influence of melt composition, *J. Geophys. Res.*, **104**, 7055-7065, (1999)
17. Frisch, U., B. Hasslacher, and Y. Pomeau. Lattice-gas automata for the Navier-Stokes equations, *Phys. Rev. Lett*., 56, 1505-1508, (1986)
18. Clague, D. S., B. D. Kandhai, R. Zhang, and P. M. A. Sloot. Hydraulic permeability of (un)bounded fibrous media using the lattice Boltzmann method, *Phys. Rev. E*, 61, 616-625, (2000)
19. Grunau, D. W., S. Y. Chen, and K. G. Eggert. A lattice Boltzmann model for multi-phase fluid flows, Phys. of Fluids A, 5(10), 2557-2562, (1993)
20. Hazlett, R. D., S. Y. Chen, and W. E. Soll. Wettability and Rate Effects on Immiscible Displacement: Lattice Boltzmann Simulation in Microtomographic Images of Reservoir Rocks. *J. of Petroleum Science and Engineering*, 20(3-4), 67-175, (1998)
21. Bhatnagar, P. L., E. P. Gross, and M. Krook. A model for collision processes in gases. I. small amplitude processes in charged and neutral one-component systems, *Phys. Rev.*, *94*, 511, (1954)
22. Chen, S. and G.D. Doolen. Lattice Boltzmann method for fluid flows. *Annu. Rev. Fluid Mech.*, 30, 329-364, (1998)
23. Bosl, W. J., J. Dvorkin, and A. Nur. A study of porosity and permeability using a lattice Boltzmann simulation, *Geophys. Res. Lett.,* 25, 1475-1478, (1998)
24. O'Connor, R. M., and J. T. Fredrich. Microscale flow modeling in geologic materials, *Phys. Chem. Earth*, 24, 611-616, (1999)
25. Ladd, A. J. C. Numerical simulations of particulate suspensions via a discretized Boltzmann equation. Part 1. Theoretical foundation, *J. Fluid Mech., 271*, 285-309, (1994)

26. McDonough, W.F. & Sun, S.-s. The composition of the earth, *Chemical Geology,* **120**, 223-253, (1995)
27. Yoshino, T., Walter, M. J. & Katsura, T. Core formation in planetesimals triggered by permeable flow, *Nature*, **422**, 154-157 (2003)
28. Yoshino, T., Walter, M. J. & Katsura, T. Connectivity of molten Fe alloy in peridotite based on in situ electrical conductivity measurements: implications for core formation in terrestrial planets, *Earth Planetary Sci. Lett.,* **222**, 625-643 (2004)
29. Kleine J., Munker, C., Mezger, K. & Palme, H. Rapid accretion and early core formation on asteroids and the terrestrials planet formation from Hf-W chronometry. *Nature,* **418***,* 952-955 (2002)
30. Minarik, B. The core of planetary formation, *Nature*, **422**, 126-128 (2003)